Selected immobilisation of individual nanoparticles by spot-exposure electron-beam-induced deposition

Daniel J. Burbridge,[1] Simon Crampin,[1] Guillaume Viau,[2] and Sergey N. Gordeev[1]

[1] *Department of Physics, University of Bath, Claverton Down, Bath BA2 7AY, United Kingdom*
[2] *Département de Génie Physique, INSA de Toulouse, 135 avenue de Rangueil, 31077 Toulouse Cedex 4, France*

The use of spot-exposure electron-beam-induced deposition (EBID) to immobilise targeted nanoparticles on a substrate is demonstrated, and investigated using experiment and simulation. Nanoparticles are secured in place through the build-up of carbonaceous material that forms in the region between a particle and substrate when an energetic electron beam is focused onto the particle and projected through to the substrate. Material build-up directly affects the strength of adhesion to the surface, and can be controlled through electron-dosage and beam energy. By selectively immobilising specific particles within surface agglomerations and removing the excess we illustrate the potential for spot-exposure EBID as a new technique for nanofabrication.

I. INTRODUCTION

The fascinating electronic, optical and mechanical properties of nanoparticles, nanotubes and nanowires make them important building blocks of modern nanotechnology.[1] A current challenge in the development of practical devices is the ability to position and secure in place nanoscale components such as these. Examples of applications where this basic requirement is key include gas sensors,[2,3] single-electron transistors,[4], nanowire field-effect transistors,[5] memory cells,[6] near-field photodetectors,[7] nanolasers ("spasers"),[8] single-plasmon sources,[9] device repair,[10] nanowire light-emitting diodes,[11] and biosensors.[12] In such hybrid devices the method of attachment of the functional nanoobject may strongly affect the device behaviour. For example, when a nanoparticle is embedded within the gap between two electrodes and attached to them via a monolayer of flexible organic molecules, it can oscillate with an amplitude of 0.1-1 nm, shuttling electrons from one electrode to the other.[13,14] However, if the nanoparticle were firmly fixed in the gap, the same structure would become a single-electron transistor with a radically different mechanism of electron transport.[15]

One method enabling the firm bonding of individual or arrays of nanoscale objects to a substrate is electron-beam-induced deposition[16,17] (EBID). In EBID, a beam of energetic (typically > 10 keV) primary electrons (PEs) is focused onto a sample. These electrons undergo multiple scattering events, resulting in backscattered electrons returning from the sample up to several microns from the point of entry of the beam. Low-energy (0–50 eV) secondary electrons (SE) are also generated in knock-on collisions, and can cause dissociation of surface-adsorbed precursor molecules, leading to the deposition of non-volatile reaction products onto the sample surface. Studies of the mechanical properties of the carbonaceous deposit that forms from the dissociation of residual hydrocarbons have shown that it can withstand a significant sheer stress[18,19], and this mechanical robustness is exploited in applications where EBID is used as a method of fixing one object to another for mechanical testing, manipulation, and to form electrical contacts.[20–24]

In these applications EBID forms a blanket of deposit covering the nanoscale objects to hold them in place.[19] Recently we have demonstrated[25,26] that due to the penetration depth of the energetic PEs used for EBID, deposit forms not only on the surfaces directly exposed to the electron beam, but also in regions of geometrical shadow, such as the underside of exposed nanoparticles and the underlying surface. Furthermore, a thin layer of deposit formed in the vicinity of the point of contact of a nanoparticle and substrate can therefore be used to secure the nanoparticle in place, with a ten-fold increase observed in the lateral force required to displace a nanoparticle following the deposition of a sub-nanometer thickness of deposit. This demonstrates the potential application of EBID for fabricating nanoparticle-containing devices by enabling the bonding of individual or arrays of nanoparticles to specific locations.

This previous work used areal-exposure, in which the electron beam scanned a region of the surface containing the nanoparticle. An undesirable consequence of this approach is the deposition of material over an extended area, which could have a detrimental effect on device behaviour. We have noted during areal-exposure experiments occasions when only nanoparticles directly exposed to the beam of PEs were sufficiently bonded to the surface to remain attached during lift-off procedures, whilst nanoparticles immediately adjacent to the exposed surface region were removed, as illustrated in Fig.1. Motivated by these observations, in the current work we pursue selective immobilisation of targeted nanoparticles through *spot-exposure* to a stationary, focused, primary electron beam, with the aim of developing a nanofabrication technique that may be used to secure nanoobjects to a surface with minimal subsidiary surface modification.

The outline of our paper is as follows. In Sec. II we describe the materials and methods used in our work, including a brief summary of the computational techniques used to simulate our EBID experiments. In Sec. III we report investigations into the deposition resulting from

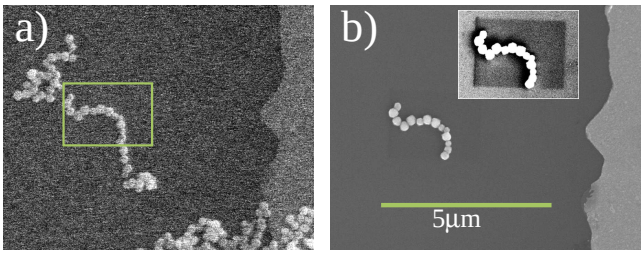

FIG. 1: Immobilisation of nanoparticles using areal-exposure EBID. a) SEM image of a group of 220 nm diameter CoNi nanoparticles on a Si substrate. The rectangle indicates the area selected for subsequent beam exposure inducing EBID (5 minute exposure with beam current of 30 pA at 30 keV with a scan rate of 0.35 s/frame). b) SEM image of the same surface region following a series of immersions in a bath of isopropyl alcohol under ultrasonic agitation. The inset shows in higher contrast the region around the remaining nanoparticles, clearly revealing the irradiated area and highlighting the correlation between exposure and attachment.

spot-exposure of an electron beam on nanoparticles, and in Sec. IV we present results demonstrating the successful targeted immobilisation of specific nanoparticles. We end with a discussion and a summary.

II. MATERIALS AND METHODS

A. Experiments

We use polycrystalline CoNi nanoparticles formed using the "polyol" process,[27] which reliably produces particles of the size employed here, which are chosen to facilitate characterisation of the deposit that forms through EBID. Seeded heterogeneous nucleation results in spherical particles with size control achieved to within 15% standard deviation from mean diameter. Two sizes and compositions are used here: 300nm diameter $Co_{50}Ni_{50}$ and 220 nm $Co_{80}Ni_{20}$ particles. The differing compositions has no consequence since Co and Ni are adjacent elements and so scatter energetic electrons similarly. Powder X-ray diffraction analysis indicates fcc CoNi solid solutions with a mean crystal size depending on particle size: 65 nm for 300 nm diameter, and 40 nm for 220 nm diameter. Each particle has a 1.8nm thick surface oxide coating,[28] the formation process producing a very clean powder with no organic coatings. Deposition onto electro-polished Si substrates was performed from suspension in iso-propyl-alcohol (IPA).

EBID was performed at room temperature using a Hitachi S-4300SE scanning electron microscope (SEM) with the vacuum pressure of the specimen chamber typically 10^{-3} Pa. Spot-exposure experiments were performed using an accelerating voltage of 30 kV and beam current of 30 pA, with the beam focused to a spot of ~ 1 nm. No precursor species were deliberately introduced to the SEM, so deposit forms solely from residual hydrocarbons in the vacuum chamber. The material deposited in this manner is known to have an amorphous structure, and consist mostly of carbon with small amounts of oxygen and hydrogen.[29] Control of deposit thickness was achieved by altering the time over which particles were exposed. In order to limit areal exposure effects we were careful to minimise imaging time both when locating particles for spot-exposure experiments, and during subsequent periodic interruptions (usually $10-30$ s intervals) during which possible drift was checked enabling the incident beam to be repositioned if necessary. Surface topography measurements were made using a Veeco MultiMode AFM with a NanoScope IIIa controller.

Forces required to laterally displace nanoparticles were also determined using the AFM, using force modulation probes (Multi75, Budgetsensors). After scanning in tapping mode to locate the desired region, an areal scan was made in contact mode while recording the horizontal Position Sensitive Detector (PSD) signal with the fast scan direction perpendicular to the cantilever's long axis (frictional force mode). Calibration was achieved by separately finding the cantilever spring constant (using the Sader method[30]) and PSD signal for cantilever twist angle. SEM measurement of the cantilever width and length, combined with the spring constant and material properties, were used to find an accurate value for cantilever thickness. This was then used to find the cantilever torsional spring constant in a similar manner to previous work.[31,32] Where possible the PSD signal was calibrated as the tip pushed against fixed particles, giving confidence in the tip's constant location. If this was not possible then the slope of friction loops was used as described by Liu et al.[33] Further details may be found in Ref. 34.

B. Simulations

Complementary computer simulation of the deposition process have been performed using Monte Carlo (MC) electron trajectory calculations[35] to determine the flux of backscattered and generated secondary electrons passing through the surfaces in the nanoparticle+substrate system. This is combined with an empirical reaction cross section[36] to determine the local rate of dissociation of hydrocarbon molecules on the surface. Dissociation results in growth of material on the surface and in a local depletion of precursor molecules, both processes that are described by a growth and diffusion model[37] that simulates the evolving surface profile in the system, along with the transport of reactant molecules.

Our Monte Carlo simulations have been described in a previous study.[26] For a large number of incident primary electrons, we calculate the subsequent trajectories as they scatter within the system along with the trajectories of generated electrons including cascades of secondaries. From these we determine the flux of secondaries passing through the surface. In the current work the

calculation is performed at regular intervals in time t as the surface profile evolves due to deposition. The simulation begins by determining the initial entry point of a PE incident from above, assuming a Gaussian beam profile with assumed width of 1 nm. Electrons are divided in "fast" electrons, with energies above 0.1 keV, and slow electrons. For fast electrons scattering is described by a modified screened Rutherford differential cross-section,[38] which governs both the angle of scattering and the mean free path which enters the Poisson-type distribution of step lengths between electron scattering events. Inelastic scattering is treated using the continuous slowing down approximation, employing a modified Bethe stopping power relation.[39]

Along each section of the fast electron trajectory SEs are generated in proportion to the energy loss per unit length using an empirically adjusted material-dependent average energy per SE. We assume SEs are emitted isotropically, using the Streitwolf excitation function to determine their energies.[40] Slow electron scattering is treated using the binary collision model[41] using an empirical mean free path between scattering events.[42] This description of the electron scattering has been shown to give a sound description of SE and backscattered electron yields over a wide range of energies, as well as a good account of the angular and energy distributions of SEs.[26]

The surface of the nanoparticle+substrate system at which growth of deposit occurs is described by a set of points $\boldsymbol{r}_S$, which evolve in time. Growth causes the surface to advance in a direction normal to the instantaneous surface profile, at a rate

$$\frac{\partial h(\boldsymbol{r}_S,t)}{\partial t} = \frac{1}{\varrho} c(\boldsymbol{r}_S,t) \int_0^{E_{\mathrm{PE}}} \sigma(E) n(E,\boldsymbol{r}_S,t) dE \qquad (1)$$

where c is the precursor concentration, ϱ is the molecular density of deposit material, σ is the cross-section for molecular dissociation, and n is the areal density of secondaries per unit energy with energy E passing through the surface at $\boldsymbol{r}_S$. We assume all carbon atoms from dissociated molecules contribute to deposit. Growth of deposit acts to deplete the local precursor concentration, which is replenished by surface diffusion:

$$\frac{\partial c(\boldsymbol{r}_S,t)}{\partial t} = D\nabla^2 c(\boldsymbol{r}_S,t) - \varrho \frac{\partial h(\boldsymbol{r}_S,t)}{\partial t}. \qquad (2)$$

Equations (1) and (2) are solved in parallel, with the distribution of secondaries found from MC electron trajectory calculations.

We find that the spectral distribution of secondaries passing through the surface in the present problem is to a good approximation independent of surface location, so that the energy integral in Eqn. (1) can be written in terms of the *total* areal density of secondaries passing through the surface at $\boldsymbol{r}_S$ and an effective cross section σ_{eff}:

$$\int_0^{E_{\mathrm{PE}}} \sigma(E) n(E,\boldsymbol{r}_S,t) dE \simeq n_{\mathrm{SE}}(\boldsymbol{r}_S,t)\sigma_{\mathrm{eff}}. \qquad (3)$$

This has the advantage that the computational effort required to accurately determine the total SE density n_{SE} in the Monte Carlo simulations is less than that required for the energy-resolved density. Finally the number of secondaries scales directly with the number of PEs, which experimentally is controlled through the beam current. Therefore we can write

$$\frac{\partial h(\boldsymbol{r}_S,t)}{\partial t} = 6.24\times10^6 \times \frac{I}{\varrho} c(\boldsymbol{r}_S,t)\widetilde{n}_{\mathrm{SE}}(\boldsymbol{r}_S,t)\sigma_{\mathrm{eff}} \qquad (4)$$

where I is the current in pA and $\widetilde{n}_{\mathrm{SE}}$ is the areal density of secondaries *per* incident primary electron.

In our simulations we use an initial surface profile corresponding to a 0.1 nm thick carbonaceous coating on a spherical nanoparticle on a planar surface. We assume the hydrocarbon precursor species is acetylene, from which the reaction cross-section[43] and calculated SE energy-distribution[26] give $\sigma_{\mathrm{eff}} = 0.014\,\mathrm{nm}^2$. The density of the carbonaceous deposit is taken to be 2 g/cm^3, which gives $\varrho = 50$ molecules/nm^3. The overall rate with which material is deposited is affected by the initial precursor concentration, which we assume is independent of position and which we use as the boundary value at large distances when solving Eqn. (2). We find values in the range 1–3 molecules/nm^2 give satisfactory agreement with experiments. These values compare with the maximum monolayer coverage expected based upon Pauling dimensions, 5 molecules/nm^2, and the value 2.8 molecules/nm^2 which has been deduced for monolayer coverage C_2H_5-Si(001),[44] where one molecule occupies each dimer site. Diffusion constants $D \sim 10^6$–10^7 nm^2/s ensure mass transport throughout the system compensating for depletion.[37] In solving Eqns. (2) and (4) we typically recalculate the SE distribution, which is tabulated on radial and angular grids for the substrate and nanoparticle respectively, every 0.1-1 s, in order to allow for the change in surface profile.

III. SPOT-EXPOSURE EBID

The distribution of EBID that forms around nanoparticles as a result of spot-exposure was studied in a series of measurements. Samples were prepared in which particles were deposited from solution onto electro-polished silicon surfaces, previously cleaned in acetone and IPA under ultrasound. This resulted in a random distribution of isolated nanoparticles or larger accumulations. Using the SEM the surface was imaged to identify suitable target particles, and for each of these the electron beam was subsequently focused onto their upper surface so that the electrons were projected through to the underlying substrate. Following exposure for a timed period topographic measurements were made using the AFM of the as-exposed nanoparticle, and then, following removal of the nanoparticle by AFM manipulation, the same area was imaged in order to observe any residual material.

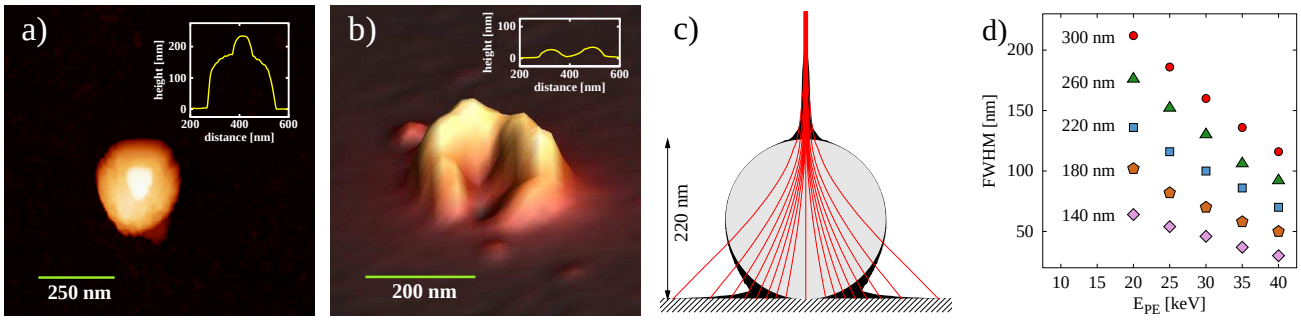

FIG. 2: a) AFM image of a nanoparticle targeted by spot-EBID. The inset shows the AFM height recorded on a cross-sectional scan, and reveals the pillar that forms above the nanoparticle. b) Image recorded following the removal of the nanoparticle by AFM manipulation, showing the presence of residual deposit. Note different colour-height scales are used in a) and b). c) Calculated distribution of deposit that forms during a simulation of spot-exposure EBID on a 220 nm diameter particle with a 30 keV PE beam. Also shown is the spread in the PE beam – moving outwards, lines indicate distances containing 0%, 10%, ... 80% of the PE flux. d) Calculated variation of the PE beam spread (FWHM) entering the substrate with beam energy, calculated for different particle sizes.

Fig. 2 shows AFM images taken when a nanoparticle has experienced spot-exposure EBID. Cross-sectional profiles taken across nanoparticles prior to exposure to the electron beam are approximately hemispherical in shape – the AFM tip cannot access beneath the nanoparticle. Images taken following spot-exposure EBID (Fig. 2a, especially inset) record a modified profile, revealing the formation of deposit on the upper surface centred on the point of focus of the PE beam in the form of a narrow pillar,[16] which occasionally broke during contact mode imaging. Note the profile in Fig. 2a includes the convoluting effects of the AFM tip. On removal of the spot-exposed nanoparticle by AFM manipulation a "cup" of material is found to remain at the original position of the particle (Fig. 2b), with a break typically observed on the side through which the particle was removed.

In simulations of the process, PEs incident upon the particle cause the generation of SEs along their trajectories, and those SEs which reach the surface have a chance of dissociating precursor molecules. The probability of SEs reaching the surface varies exponentially with depth, with a decay length (often called "the escape depth") that we calculate to be 3 nm for carbon. This relatively shallow depth means it is the distribution of PEs near the surfaces of the system that essentially determine the formation of deposit. We calculate the maximum penetration range of 30 keV electrons in CoNi to be 2.8μm, meaning a 220 nm diameter nanoparticle appear almost transparent to the PE beam. Hence as well as growth occurring in the vicinity of the entry point of the PE beam into the nanoparticle, which results in the nanopillar forming, growth can also take place near where the beam exits. In passing through the nanoparticle, the incident PEs undergo scattering events in which their direction of propagation is altered, resulting in broadening of the initially collimated beam, shown in Fig. 2c. We find an initially collimated beam of 30 keV PEs exits a 220 nm diameter nanoparticle with a full-width half-maximum (FWHM) spread of $\sim 30^\circ$, corresponding to a FWHM radial spread of 100 nm as it enters the substrate, Fig. 2d. This broadening is important as the PE beam spread determines the distribution of secondaries, and consequently the region over which carbonaceous deposit forms. The simulations show that deposit develops on both the lower surface of the nanoparticle as well as the substrate beneath it. In each of the growth regions, the SEs that dissociate precursor molecules originate from both the nanoparticle and the substrate.

AFM images of the topography of the surface recorded following nanoparticle removal (Fig. 2b) show a distribution of material that resembles that of the deposit which builds up on the substrate in our simulations. This suggests that adhesion between the deposit and the particle is weaker than between the deposit and the Si substrate, so that during displacement fracture occurs at the interface between the particle and the carbonaceous deposit, thereby leaving material that corresponds to the deposit that existed on the substrate. To further investigate the systematics of the growth and the effect of the deposit we selected a line of particles, shown in Fig. 3, and performed a series of spot-exposures on alternate particles applying different electron doses, using an exposure duration of 50 s for the upper particle and then successively 40, 30, 20, and finally 10 seconds for the lower particle. We adopt this procedure to limit as much as possible variations in conditions other than electron dose, that might otherwise affect the growth (for example, being reliant upon residual hydrocarbon contamination to provide precursor material we observe day-to-day variation in the amount of residual deposit found following the removal of nanoparticles that have experienced similar electron doses). After imaging the line of particles following exposure (Fig. 3a), the area was scanned with the AFM in contact mode to sweep away the particles. A tapping mode AFM image of the region following particle removal is shown in in Fig. 3b.

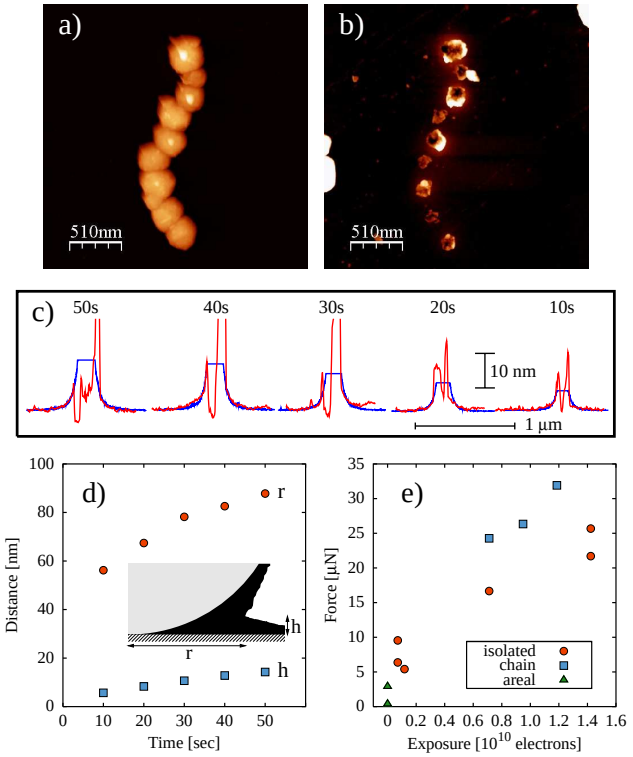

FIG. 3: Systematic study of deposition formed during spot-exposure EBID. (a) AFM image of a chain of nanoparticles following spot-exposure EBID. Alternate particles starting with the uppermost were exposed for 50, 40, 30, 20 and 10s respectively. (b) Image of residual deposit following removal of nanoparticles by contact-mode AFM. (c) Topographic cross-sections of the residual deposit in (b) taken along scan-lines passing through the locations of the targeted nanoparticles (red), along with calculated deposition profiles (blue). The simulation results are truncated to only show the profile beneath the "neck" of the deposit that forms. (d) Evolutions of the radial distance (r) and height (h) of the neck of deposit material formed during simulations of the deposition process – the inset shows a close-up of the region around the base of the nanoparticle (see Fig. 2c). (e) Forces required to displace nanoparticles immobilised by different electron doses in EBID. For the areal exposure data the electron dose is taken to be the number of electrons intersecting the cross-sectional area of the nanoparticle.

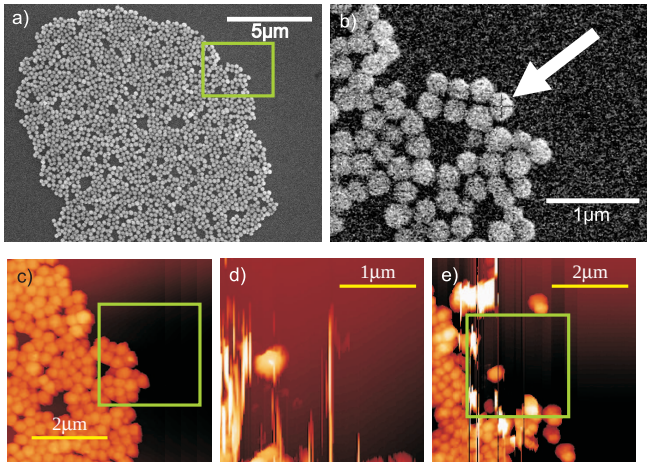

FIG. 4: a) SEM image of a raft of 300 nm diameter particles deposited on a Si surface. The rectangle indicates the area of image b). b) SEM close up of the raft shown in a), with the particle targeted for spot-exposure indicated. c) AFM tapping mode image showing distribution of particles following spot-exposure EBID applied to target particle. d) Height-data obtained during contact mode scan over region indicated in c). e) As c) but following contact mode scan.

In Fig. 3c we compare the measured profiles of the residual deposit (line scans from Fig. 3b taken across the original locations of the spot-exposed particles) with snapshots of the evolving profile that forms in a simulation. The agreement confirms our interpretation that the material remaining following particle removal reveals the distribution of deposit that forms during the EBID process. The measured heights of the residual material are very irregular, due to variation in the point of fracture. The simulations show more clearly how the extent of the deposit increases with the electron dose (equivalent to time in our experiments/simulations), Fig. 3d. Using the position of the "neck" as a reference point, the height increases approximately linearly with electron dose, and the radial extent shows an initial rapid rise and then a slower increase, due to the geometrical nature of the growth fronts.

Data for the forces that were required to displace nanoparticles following EBID are shown in Fig. 3d. Only data for the particles in the chain exposed for 50, 40 and 30 s were obtained – the AFM sweep moved from the top to the bottom of Fig. 3a, and in the course of the sweep the tip picked up material that affected the forces obtained from the particles exposed for 20 and 10 s. However Fig. 3d also contains additional force data obtained from isolated particles that were on the same sample, and that were targeted by spot-exposure EBID in the same exposure run, as the chain system, as well as values for the forces required to remove particles fixed with an areal exposure. The results demonstrate a general linear increase in adhesion with electron dose. We attribute the consistently larger forces that were required to displace the particles in Fig. 3a, compared to the isolated particles, on the greater amount of imaging performed on these particles, undertaken in order to position subsequent spot exposures. This additional exposure is not included in the electron dosage value used. We believe that this imaging also accounts for the regions of deposit that may be seen in Fig. 3b to have formed beneath particles which were not directly exposed to a spot exposure.

IV. TARGETED IMMOBILISATION

The preceeding results demonstrate that individual nanoparticles can be targeted and immobilised through

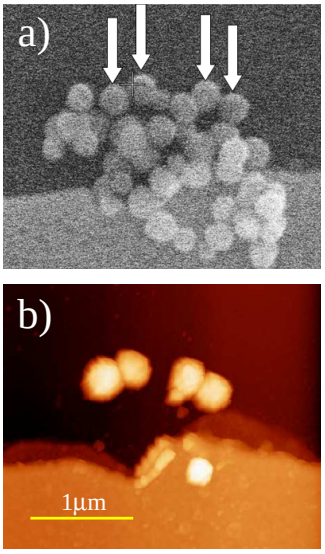

FIG. 5: a) SEM image showing an accumulation of 300 nm particles on a Si surface with a gold photolithographic mark. Arrows are used to identify the four particles selected for spot-exposure EBID. b) Tapping mode AFM image of the same surface region following the exposure run and treatment by ultrasonic agitation in IPA to remove excess.

spot-exposure EBID, with the forces required to displace them being many times greater than that required for non-exposed particles. In order to demonstrate the selective nature of the spot-exposure EBID-immobilisation, a monolayer raft of particles was deposited as shown in Fig. 4a. The particle indicated in the magnified view in Fig. 4b was exposed to a spot exposure with a dose of 1.3×10^{10} electrons. The nanopillar that formed on top of the particle can just be made out in the tapping mode AFM image subsequently taken, Fig. 4c. The AFM was then engaged in contact mode and scanned over an area surrounding the targeted particle in order to sweep aside the non-immobilised particles. Height data acquired during this scan shown in Fig. 4d demonstrates that only the targeted particle remained stationary during the sweep, with the additional noise being due to the displacement of non-attached particles. Fig. 4e is a further tapping mode image taking after sweep-away, showing the surface region surrounding the targeted particle is clear.

Although using the AFM to remove particles in this manner is effective at clearing the scanned area, it is limited by the scan range of the AFM and this results in an accumulation of particles at the edges of the scanned area, which can be seen in Fig. 4e. An alternative experiment was performed, in which four particles in the agglomeration in Fig. 5a were selected for spot-exposure EBID, following which the sample underwent a treatment of ultrasonic agitation in IPA. As previously evidenced by Fig. 1 this method is effective at removing particles from large areas, and as can be seen from Fig. 5b the non-exposed particles have been removed whilst the targeted particles remain in place.

V. DISCUSSION

The results presented in Sections III and IV illustrate the application of spot-exposure EBID to immobilise individual nanoparticles, which are secured in place through the build-up of material that forms around the point of contact of nanoparticle and substrate when an electron beam is projected through the particle. Using this technique we have succeeded in immobilising target particles amongst larger accumulations, removing non-targeted particles either by using the AFM tip to sweep them away or using an ultrasonic bath.

Measurements of the residual deposit following particle removal and comparison with simulations indicates that the build-up of material can be controlled by the electron dose. Accompanying increased deposit is an increase in the force required to subsequently displace the particles, confirming the ability to manipulate the attachment of particles to substrates. The forces that we obtain are as much as 100 times the force required to displace a non-exposed particle,[26] indicating that this technique could find use in securing particles that will subsequently be exposed to a wide range of environments or conditions.

Our studies have been performed on $200 - 300$ nm diameter CoNi particles, but the mechanisms are generally valid for other compositions and particle sizes. (One possible exception may be insulating substrates, where charging could be an issue.) We expect smaller particles will require less deposit to secure them in place. As seen in Fig. 2d smaller particle size naturally leads to a narrower spread of PE electrons exiting the lower surface and entering the substrate, which itself influences the distribution of SEs and consequently the deposition of material that fixes the particle in place. Thus it should be possible to continue to ensure that material build-up is strongly localised to the area beneath the nanoparticle, confirmed by simulation. Fig. 2d also shows that varying the beam energy provides additional control. Beam attenuation is greater at lower energies, and so a compensatory increase in electron dosage will need to be employed to achieve a certain thickness of deposit. Finally, lighter elements result in narrower PE beam spread which can be compensated for through the use of lower energy. For example, for Si nanoparticles of a given diameter we find that the beam spread at 10 keV is comparable to that found at 40keV for CoNi nanoparticles of similar size (reported in Fig. 2d).

Compared to particle immobilisation using areal-exposure EBID, using a spot-exposure results in less widespread build-up of deposit on the nanoparticle, and elsewhere on the substrate. This “contamination” is largely restricted to the formation of a nanopillar at the point of entry of the electron beam into the nanoparticle, whereas areal-exposure EBID results in an almost uniform coating on the nanoparticle and substrate (compare Fig. 2c with Fig. 6 in Ref. 26). This different distribution of deposit could account for the different failure mechanism that occurs when secured parti-

cles are forcibly displaced — here we observe adhesion between particle and deposit to fail, whereas following areal exposure[26] we found adhesion between deposit and substrate to fail.

By comparing the results of simulations with those in which the formation of the nanopillar is artificially suppressed (by setting to zero the SE passing through the upper surface region of the nanoparticle), we find that the pillar does not greatly affect the formation of deposit beneath the particle, having only a slight overall effect on the PE beam width and intensity as it exits the nanoparticle. However the nanopillar does acts as a source of SEs. The growth area beneath the nanoparticle is shielded from these by the nanoparticle itself, but they are able to reach more distant areas of the substrate and cause the formation of deposit. Thus nanopillar formation can be regarded as generally undesirable. Growth of the pillar can be suppressed relative to the region beneath the nanoparticle by increasing the beam current so that deposition takes place within a diffusion-limited regime. Then the flow of precursor molecules from the substrate to the upper parts of the nanoparticle is inhibited by greater probability of dissociation as molecules flow through the growth area beneath the particle.

Possible applications of the technique of selective spot-exposure EBID to fix nanoparticles in place described in this paper would be in making arrays of nanoparticles required, for example, for plasmonic waveguides.[45] The fabrication may start with self-assembly of a monolayer of nanoparticles in the required area of the substrate. SEM imaging of the monolayer can be used to determine exact positions of the nanoparticles, taking care to avoid excessive electron dosage that might fix all particles. This may impose some constrains on the imaging duration, electron-beam current or the vacuum environment. After imaging, the required pattern can be formed by spot-exposure of selected nanoparticles with the focused electron beam, with unsecured nanoparticles then being removed by ultrasonic agitation in IPA. The method could be applied repeatedly in order to make more complex patterns containing different types of nanoobjects (nanotubes, nanorods etc.), or nanoparticles of different sizes.

VI. SUMMARY

To summarise, the use of spot-exposure electron-beam-induced deposition to immobilise targeted nanoparticles on a substrate has been demonstrated, and investigated using experiment and simulation. Nanoparticles are secured in place through the build-up of material that forms in the region between particle and substrate when an energetic electron beam is focused onto the particle and projected through to the substrate, with generated electrons dissociating residual hydrocarbons resulting in carbonaceous deposit. Computer simulations have been used to identify the extent of this deposit, which is primarily governed by electron scattering within the nanoparticle. Material build-up, which directly affects adhesion to the surface, may be controlled through electron-dosage and beam energy. We have applied this technique using a 30 keV electron beam to target individual $200 - 300$ nm diameter CoNi particles within accumulations, immobilising them on Si surfaces with non-targeted particles removed using either an AFM or ultrasonic agitation. Although we have considered this specific system, the approach may be adapted to other materials and particle sizes, opening up a new technique for use in nanofabrication.

VII. ACKNOWLEDGEMENTS

DJB acknowledges the support of the UK EPSRC through the award of a DTA studentship.

[1] V. M. Rotello, *Nanoparticles: building blocks for nanotechnology* (Springer, 2003).

[2] G. K. Mor, O. K. Varghese, M. Paulose, and C. A. Grimes, Sensor Letters **1**, 42 (2003).

[3] O. Lupan, L. Chow, and G. Chai, Sensors and Actuators B **141**, 511 (2009).

[4] C. Thelander, M. H. Magnusson, K. Deppert, L. Samuelsen, P. R. Poulsen, J. Nygard, and J. Borggren, Applied Physics Letters **70**, 2106 (2001).

[5] K. Keem, J. Kang, C. Yoon, D. Yeom, D. Jeong, B. Moon, and S. Kim, Microelectronic Engineering **84**, 1622 (2007).

[6] C. S. Wu, C. D. Chen, S. M. Shih, and W. F. Su, Applied Physics Letters **81**, 4594 (2002).

[7] M. Hegg and L. Y. Lin, Optics Express **15**, 17163 (2007).

[8] M. A. Noginov, G. Zhu, A. M. Belgrave, R. Bakker, V. M. Shalaev, E. E. Narimanov, S. Stout, E. Herz, T. Suteewong, and U. Wiesner, Nature **460**, 1110 (2009).

[9] A. Falk, F. H. L. Koppens, C. L. Yu, N. L. Snapp, A. A. V., M. Jo, M. D. Lukin, and H. Park, Nature Physics **5**, 475 (2009).

[10] I. Utke, B. Dwit, C. F, P. Hoffmann, and K. E, Microelectronic Engineering **53**, 261 (2000).

[11] A. Motayed, A. V. Davydoc, M. He, S. N. Mohammad, and J. Melngailis, Applied Physics Letters **90**, 183120 (2007).

[12] X. Luo, A. Morrin, A. J. Killard, and M. R. Smyth, Electroanalysis **18**, 319 (2006).

[13] L. Y. Gorelik, A. Isacsson, M. V. Voinova, B. Kasemo, R. I. Shekhter, and M. Jonson, Physical Review Letters **80**, 4526 (1998).

[14] A. V. Moskalenko, S. N. Gordeev, O. F. Koentjoro, P. R. Raithby, R. W. French, F. Marken, and S. E. Savel'ev, Physical Review B **79**, 241403 (2009).

[15] N. Nishiguchi, Physical Review B **65**, 035401 (2001).

[16] N. Silvis-Cividjian and C. W. Hagen, *Electron-beam-induced nanometer-scale deposition*, vol. 143 of *Advances in Imaging and Electron Physics* (Elsevier, 2006).

[17] W. F. van Dorp and C. W. Hagen, Journal of Applied Physics **104**, 081301 (2008).

[18] K. Molhave, D. N. Madsen, S. Dohn, and P. Boggild, Nanotechnology **15**, 1047 (2004).

[19] W. Ding, D. A. Dikin, X. Chen, R. D. Piner, R. S. Ruoff, E. Zussman, X. Wang, and X. Li, Journal of Applied Physics **98** (2005).

[20] M. F. Yu, O. Lourie, M. J. Dyer, K. Moloni, T. F. Kelly, and R. S. Ruoff, Science **287**, 637 (2000).

[21] D. Bozovic, M. Bockrath, J. H. Hafner, C. M. Lieber, H. Park, and M. Tinkham, Physical Review B **67** (2003).

[22] D. N. Madsen, K. Molhave, R. Mateiu, A. M. Rasmussen, M. Brorson, C. J. H. Jacobsen, and P. Boggild, Nano Letters **3**, 47 (2003).

[23] E. Zussman, X. Chen, W. Ding, L. Calabri, D. A. Dikin, J. P. Quintana, and R. S. Ruoff, Carbon **43**, 2175 (2005).

[24] O. Lupan, G. Chai, and L. Chow, Microelectronic Engineering **85**, 2220 (2008).

[25] A. V. Moskalenko, D. J. Burbridge, G. Viau, and S. N. Gordeev, Nanotechnology **18**, 025304 (2007).

[26] D. J. Burbridge, S. Crampin, G. Viau, and S. N. Gordeev, Nanotechnology **19**, (2008).

[27] P. Toneguzzo, G. Viau, O. Acher, F. Fievet-Vincent, and F. Fievet, Advanced Materials **10**, 1032 (1998).

[28] P. Toneguzzo, G. Viau, O. Acher, F. Guillet, E. Bruneton, F. Fievet-Vincent, and F. Fievet, Journal of Materials Science **35**, 3767 (2000).

[29] T. Bret, S. Mauron, I. Utke, and P. Hoffmann, Microelectronic Engineering **78-79**, 300 (2005).

[30] J. E. Sader, J. W. M. Chon, and P. Mulvaney, Review of Scientific Instruments **70**, 3967 (1999).

[31] D. Choi, W. Hwang, and E. Yoon, Journal of Microscopy-Oxford **228**, 190 (2007).

[32] H. Xie, J. Vitard, D. S. Haliyo, and S. Regnier, Ieee Sensors Journal **8**, 1478 (2008).

[33] Y. Liu, D. F. Evans, Q. Song, and D. W. Grainger, Langmuir **12**, 1235 (1996).

[34] D. J. Burbridge, Phd thesis, University of Bath (2009).

[35] D. C. Joy, *Monte Carlo Modeling for Electron Microscopy and Microanalysis* (Oxford University Press: New York, 1995).

[36] N. Silvis-Cividjian, C. W. Hagen, and P. Kruit, Journal of Applied Physics **98** (2005).

[37] K. Rykaczewski, W. B. White, and A. G. Fedorov, Journal of Applied Physics **101** (2007).

[38] D. Liljequist, F. Salvat, R. Mayol, and J. D. Martinez, Journal of Applied Physics **65**, 2431 (1989).

[39] D. C. Joy and S. Luo, Scanning **11**, 176 (1989).

[40] H. W. Streitwolf, Ann. Phys. (Leipz.) **3**, 183 (1959).

[41] Koshikaw.T and R. Shimizu, Journal of Physics D-Applied Physics **7**, 1303 (1974).

[42] M. P. Seah and W. A. Dench, Surface and Interface Analysis **1**, 2 (1979).

[43] D. A. Alman, D. N. Ruzic, and J. N. Brooks, Physics of Plasmas **7**, 1421 (2000).

[44] P. A. Taylor, R. M. Wallace, C. C. Cheng, W. H. Weinberg, M. J. Dresser, W. J. Choyke, and J. T. Yates, J. Am. Chem. Soc. **114**, 6754 (1992).

[45] S. A. Maier, P. G. Kik, H. A. Atwater, S. Meltzer, E. Harel, B. E. Koel, and A. A. G. Requicha, Nature Materials **2**, 229 (2003).